

Special breathing structures induced by bright solitons collision in a binary dipolar Bose—Einstein condensates

Gen Zhang(张根), Li-Zheng Lv(吕李政), Peng Gao(高鹏), and Zhan-Ying Yang(杨战营)
Citation: Chin. Phys. B, 2023, 32 (**11**): 110303. DOI: 10.1088/1674-1056/acf283
Journal homepage: http://cpb.iphy.ac.cn; http://iopscience.iop.org/cpb

What follows is a list of articles you may be interested in

Gap solitons of spin-orbit-coupled Bose-Einstein condensates in $\mathcal{PT}$ periodic potential

S Wang(王双), Y H Liu(刘元慧), and T F Xu(徐天赋)
Chin. Phys. B, 2022, 31 (**7**): 070306. DOI: 10.1088/1674-1056/ac538e

Quantum reflection of a Bose-Einstein condensate with a dark soliton from a step potential

Dong-Mei Wang(王冬梅), Jian-Chong Xing(邢健崇), Rong Du(杜荣), Bo Xiong(熊波), and Tao Yang(杨涛)
Chin. Phys. B, 2021, 30 (**12**): 120303. DOI: 10.1088/1674-1056/ac051e

Dynamics of bright soliton in a spin-orbit coupled spin-1 Bose-Einstein condensate

Hui Guo(郭慧), Xu Qiu(邱旭), Yan Ma(马燕), Hai-Feng Jiang(姜海峰), and Xiao-Fei Zhang(张晓斐)
Chin. Phys. B, 2021, 30 (**6**): 060310. DOI: 10.1088/1674-1056/abf34a

Spin-orbit-coupled spin-1 Bose-Einstein condensates confined in radially periodic potential

Ji Li(李吉), Tianchen He(何天琛), Jing Bai(白晶), Bin Liu(刘斌), and Huan-Yu Wang(王寰宇)
Chin. Phys. B, 2021, 30 (**3**): 030302. DOI: 10.1088/1674-1056/abc53e

Interference properties of two-component matter wave solitons

Yan-Hong Qin(秦艳红), Yong Wu(伍勇), Li-Chen Zhao(赵立臣), Zhan-Ying Yang(杨战营)
Chin. Phys. B, 2020, 29 (**2**): 020303. DOI: 10.1088/1674-1056/ab65b7

SPECIAL TOPIC — Celebrating the 100th Anniversary of Physics Discipline of Northwest University

Special breathing structures induced by bright solitons collision in a binary dipolar Bose–Einstein condensates

Gen Zhang(张根)[1,2], Li-Zheng Lv(吕李政)[1,2], Peng Gao(高鹏)[3], and Zhan-Ying Yang(杨战营)[1,2,4,†]

[1] *School of Physics, Northwest University, Xi'an* 710127, *China*
[2] *Shaanxi Key Laboratory for Theoretical Physics Frontiers, Xi'an* 710127, *China*
[3] *Graduate School, China Academy of Engineering Physics, Beijing* 100193, *China*
[4] *Peng Huanwu Center for Fundamental Theory, Xi'an* 710127, *China*

(Received 30 June 2023; revised manuscript received 12 August 2023; accepted manuscript online 22 August 2023)

We numerically investigate the breathing dynamics induced by collision between bright solitons in a binary dipolar Bose–Einstein condensates, whose dipole–dipole interaction and contact interaction are attractive. We identify three special breathing structures, such as snakelike special breathing structure, mixed breathing structure, and divide breathing structure. The characteristics of these breathing structures can be described by breathing frequency Ω, maximum breathing amplitude A and lifetime τ, which can be manipulated by atomic number N_i and interspecies scattering length a_{12}. Meanwhile, the above breathing structures can realize the process of quasi-transition with a reasonable N_i and a_{12}. Additionally, the collision of two special breathing structures also can bring more abundant breathing dynamics. Our results provide a reference for the study of soliton interactions and deepen the understanding of soliton properties in a binary dipolar Bose–Einstein condensates.

Keywords: dipolar Bose–Einstein condensates, soliton, soliton collision

PACS: 03.75.Mn, 05.45.–a, 34.50.Cx **DOI:** 10.1088/1674-1056/acf283

1. Introduction

The interaction between solitons has always been a hot topic in research due to its rich dynamical behavior.[1–8] The phase shift that occurs after elastic collision between solitons reveals the nature of particle-like.[4,5] The theoretical analysis of the interaction between bright solitons in potential wells has led to the observation of interference patterns.[8] In recent years, the realization of dipolar Bose–Einstein condensates (BECs) has provided a new direction for studying soliton interactions.[9–15] The atoms that make up dipolar BECs have large magnetic dipole moment, which gives rise to the occurrence of dipole–dipole interactions. Dipole–dipole interaction is an anisotropic long-range interaction, which is fundamentally different from the isotropic short-range contact interaction.[16–22] The long-range feature of dipole–dipole interactions allows for the stabilization of multidimensional solitons and new local waves (such as soliton molecules and dark solitons with ripples[23–26]), while the anisotropic feature facilitates the formation of anisotropic solitons (such as anisotropic bright and vortex solitons[27,28]). Therefore, exploring the nonlinear excitation dynamics under dipole–dipole interactions is an important topic in ultracold atom systems.

The extensive research has been conducted on the interaction between solitons in finite-component systems. In single-component BECs systems, the formation and propagation of bright solitons in ^{7}Li atoms,[29,30] as well as the collision dynamics between these solitons,[2] have been studied extensively. Compared with single-component BECs, multi-component BECs exhibit richer dynamics as they not only have intraspecies interactions but also have interspecies interactions.[19,31–33] For example, vector solitons such as bright–bright solitons[34–36] and dark–dark solitons[37,38] have been theoretically predicted in multi-component BECs.

As we know, there has been a lack of research on soliton interactions in multi-component dipolar BECs systems. Therefore, the study of soliton collision dynamics in this system is worthy of more attention. There are some important unresolved issues. (i) In single-component dipolar BECs, soliton interactions lead to breathing phenomena. Can multi-component dipolar BECs bring more various dynamic phenomena? (ii) How to control these nonlinear excitations and characterize their regularity? Based on these questions, our research is carried out.

In this paper, we investigate the interaction between solitons in a binary dipolar BECs system. The numerical results indicate that the collision of two bright solitons can induce special breathing structures, such as snakelike special breathing structure (SS), mixed breathing structure (MS), and divided breathing structure (DS). We have demonstrated that the existence of these three special breathing structures depends on traditional breathing solitons (TS). And their breath-

†Corresponding author. E-mail: zyyang@nwu.edu.cn

© 2023 Chinese Physical Society and IOP Publishing Ltd

ing properties are closely related to the atomic number N_i and interspecies scattering length a_{12}. Meanwhile, we find that the lifetime of the MS structure can also be manipulated by atomic number N_i and interspecies scattering length a_{12}. In addition, the collision between these special breathing structures can also bring some interesting dynamics. After the collision of SS and DS structures of the same type, they can maintain their own stability. When two MS structures of the same type collide, they exhibit different breathing dynamics at different velocities. Our research results demonstrate that collisions between bright solitons in a binary dipolar BECs system lead to richer breathing dynamics, providing a reference for future studies of solitons and their interactions in multi-component dipolar BECs systems.

2. Model of the binary dipolar BECs

The dynamics of binary dipole BECs can be described by the coupled Gross–Pitaevskii (GP) model[22,39,40]

$$\mathrm{i}\hbar\frac{\partial\Psi_1}{\partial t}=\Big[-\frac{\hbar^2}{2m_1}\nabla^2+V_1(\boldsymbol{r})+\frac{4\pi\hbar^2}{m_1}a_1N_1|\Psi_1|^2+\frac{2\pi\hbar^2}{m_{\mathrm{R}}}a_{12}N_2|\Psi_2|^2+\frac{N_1\mu_0}{4\pi}\Phi_{\mathrm{dd}}{}^{(1)}+\frac{N_2\mu_0}{4\pi}\Phi_{\mathrm{dd}}{}^{(12)}\Big]\Psi_1, \quad (1)$$

$$\mathrm{i}\hbar\frac{\partial\Psi_2}{\partial t}=[-\frac{\hbar^2}{2m_2}\nabla^2+V_2(\boldsymbol{r})+\frac{4\pi\hbar^2}{m_2}a_2N_2|\Psi_2|^2+\frac{2\pi\hbar^2}{m_{\mathrm{R}}}a_{12}N_1|\Psi_1|^2+\frac{N_2\mu_0}{4\pi}\Phi_{\mathrm{dd}}{}^{(2)}+\frac{N_1\mu_0}{4\pi}\Phi_{\mathrm{dd}}{}^{(21)}]\Psi_2, \quad (2)$$

we consider a bright soliton in a binary dipole BECs whose mass, atomic number, and scattering length for the two species $i=1,2$, given by m_i, N_i and a_i, respectively. $\Psi_i(\boldsymbol{r},t)$ is the mean-field wave function of condensates. The third and fourth terms on the right side of the equation represent intraspecies and interspecies contact interactions, and the fifth and sixth terms represent intraspecies and interspecies dipole interactions. Here a_{12} represents the interspecies scattering length, μ_0 is the permeability of the free space, and $m_{\mathrm{R}}=m_1m_2/(m_1+m_2)$ is the reduced mass. The external potential $V_i(\boldsymbol{r})$ provides a trap where the cloud is confined, and it can be assumed as a harmonic form, $V_i(\boldsymbol{r})=m_i\omega_i{}^2\rho^2$, where ω_i is the angular frequencies of the traps acting on the two species in the transverse ρ direction (here, $\omega_1=\omega_2$). Meanwhile, axial trap is ignored. The nonlocal dipolar potential is

$$\Phi_{\mathrm{dd}}{}^{(ij)}=\int\frac{\mu_i\mu_j(1-3\cos\theta)}{|(\boldsymbol{r}-\boldsymbol{r}')|^3}\Psi_j(\boldsymbol{r}',t)\,\mathrm{d}\boldsymbol{r}', \quad \rho^2=x^2+y^2,$$

where θ is the angle between the vector joining interacting particles and the dipole direction, μ_i and μ_j are the magnetic dipole moment. Under the action of the transverse external trap $V_i(\boldsymbol{r})$, the condensates are compressed to be cigar-shaped, so that we can consider them to be a quasi-one-dimensional dipolar BECs. The 3D model can be reduced into a 1D model. For this purpose, we can assume a wave function $\Psi_i(\boldsymbol{r},t)=\psi_i(z)\phi_i(x,y)\exp[-\mathrm{i}t(m_i\omega_i^2l_i^2)/\hbar]$, where $\phi_i(x,y)=\exp[-(x^2+y^2)/(2l_i^2)]/(l_i\sqrt{\pi})$ and $l_i=\sqrt{\hbar/(m_i\omega_i)}$. By the integration over transverse directions, the effective 1D potential of the dipole–dipole interaction is obtained as

$$\tilde{\Phi}_{\mathrm{dd}}^{(ij)}(z,t)=-\frac{\alpha\mu_i\mu_j}{2{l_1}^3}\int_{-\infty}^{+\infty}\tilde{R}(z-z')\left|\tilde{\psi}_j(z',t)\right|^2\mathrm{d}z',$$

where $\alpha=(1+3\cos\theta)/4$ with a range from $-1/2$ to 1, and θ is the angle between dipole and z direction. The nonlocal response function has the form of $\tilde{R}(z)=(1+2u^2)\exp(u^2)\mathrm{erfc}(|u|)-2\pi^{-1/2}|u|$, where $u=z/(\sqrt{2}l_1)$ and erfc is the complementary error function (the detailed calculation of the 1D dipolar potential has been illustrated in Ref. [41]). Then, by the transformation

$$t=\frac{2}{\omega_1}T,\ \ z=\sqrt{2}l_1Z,\ \ \tilde{\psi}_i=-\frac{1}{2\sqrt{|a_{\mathrm{s}0}|}}\psi_i,$$

we can transform the 1D binary dipolar model into a dimensionless model. For convenience, the labels Z and T are severally replaced by z and t, and the final dimensionless model becomes

$$\begin{aligned}\mathrm{i}\psi_{1t}=&-\frac{1}{2}\psi_{1zz}+g_{\mathrm{c}}^{(1)}|\psi_1|^2\psi_1+g_{\mathrm{c}}{}^{(12)}|\psi_2|^2\psi_1\\&+g_{\mathrm{d}}{}^{(1)}\int R(z-z')\left|\psi_1(z',t)\right|^2\mathrm{d}z'\psi_1\\&+g_{\mathrm{d}}{}^{(12)}\int R(z-z')\left|\psi_2(z',t)\right|^2\mathrm{d}z'\psi_1, \quad (3)\\ \mathrm{i}\psi_{2t}=&-\frac{m_1}{2m_2}\psi_{2zz}+g_{\mathrm{c}}^{(2)}|\psi_2|^2\psi_2+g_{\mathrm{c}}{}^{(21)}|\psi_1|^2\psi_2\\&+g_{\mathrm{d}}{}^{(2)}\int R(z-z')\left|\psi_2(z',t)\right|^2\mathrm{d}z'\psi_2\\&+g_{\mathrm{d}}{}^{(21)}\int R(z-z')\left|\psi_1(z',t)\right|^2\mathrm{d}z'\psi_2, \quad (4)\end{aligned}$$

where the response function is

$$R(z)=(1+2z^2)\exp(z^2)\mathrm{erfc}(|z|)-2\pi^{-1/2}|z|.$$

In this equation,

$$g_{\mathrm{c}}^{(1)}=\frac{200\hbar a_1}{3m_1l_1^2\omega_1|a_{\mathrm{s}0}|},\ \ g_{\mathrm{c}}^{(2)}=\frac{200\hbar a_2}{3m_2l_2^2\omega_1|a_{\mathrm{s}0}|},$$

$$g_{\mathrm{c}}^{(12)}=\frac{100\hbar a_{12}}{m_{\mathrm{R}}(2l_1^2+l_2^2)\omega_1|a_{\mathrm{s}0}|},\ \ g_{\mathrm{c}}^{(21)}=\frac{100\hbar a_{12}}{m_{\mathrm{R}}(l_1^2+2l_2^2)\omega_1|a_{\mathrm{s}0}|},$$

$$g_{\mathrm{d}}^{(1)}=\frac{-25\sqrt{2}\alpha\mu_0\mu_1^2}{4\pi\hbar\omega_1l_1^2|a_{\mathrm{s}0}|},\ \ g_{\mathrm{d}}^{(2)}=\frac{-25\sqrt{2}\alpha\mu_0\mu_2^2l_1}{4\pi\hbar\omega_1l_2^3|a_{\mathrm{s}0}|},$$

$$g_{\mathrm{d}}^{(12)}=\frac{-25\sqrt{2}\alpha\mu_0\mu_1\mu_2l_1}{4\pi\hbar\omega_1l_2^3|a_{\mathrm{s}0}|},\ \ g_{\mathrm{d}}^{(21)}=\frac{-25\sqrt{2}\alpha\mu_0\mu_1\mu_2}{4\pi\hbar\omega_1l_1^2|a_{\mathrm{s}0}|},$$

where $g_{\mathrm{c}}^{(i)}$ and $g_{\mathrm{d}}^{(i)}$ represent the strength of intraspecies contact and intraspecies dipolar interactions, respectively. $g_{\mathrm{c}}^{(ij)}$ and $g_{\mathrm{d}}^{(ij)}$ represent the strength of interspecies contact and interspecies dipolar interactions, $a_{\mathrm{s}0}$ is the background value of

scattering length. The positive(or negative) values of g_c and g_d indicate the repulsive(or attractive) interaction.

In our numerical simulations, the binary dipolar condensates of ^{164}Dy and ^{168}Er atoms are considered, which have the largest magnetic moments of all the dipolar atoms used in the BECs experiments. For the ^{164}Dy–^{168}Er mixture, we label ^{164}Dy atoms as $i=1$, and ^{168}Er atoms as $i=2$. The magnetic moment of a ^{164}Dy atom is $\mu_1 = 10\mu_B$[9] and of a ^{168}Er atom is $\mu_2 = 7\mu_B$[10] with μ_B being the Bohr magneton. We have $m_1 = 2.72329\times10^{-25}$ kg, $m_2 = 2.78971\times10^{-25}$ kg, $l_1 = 1$ μm, $l_2 = 0.99$ μm, $\omega_1 = \omega_2 = 2\pi\times61$ Hz, $\mu_B = 9.27401\times10^{-24}$ A·m^2, $\mu_0 = 4\pi\times10^{-7}$ N·A^{-2}, $\hbar = 1.05457\times10^{-34}$ J·s, $a_{s0} = 1.17\times10^{-7}$ m, and $a_0 = 5.292\times10^{-11}$ m with a_0 being the Bohr radius. Since the values of m_1 and m_2 are relatively close, we also approximate the coefficient of the kinetic energy term of model (4) to $-1/2$. The units of space and time coordinates are respectively $x_u = \sqrt{2}l_1 = 1.414$ μm and $t_u = 2/\omega_1 = 5.22$ ms. The realistic atom number is $\tilde{N}_i = N_i\sqrt{2}l_1/(4|a_{s0}|) = 30218N_i$, where N_i is the dimensionless one.

The experimental values of the scattering lengths we considered are all known, except for the intraspecies scattering length of ^{168}Er atoms. Preliminary cross-dimensional thermalization measurements indicate that the scattering length is between $150a_0$ and $200a_0$.[10] The scattering length can be experimentally controlled independently by magnetic[42] and optical[43] Feshbach resonance techniques. The dipole interaction strength g_d can be changed by adjusting α. In contrast to single-component dipolar BECs, binary dipolar BECs not only have intraspecies interactions but also have dipole–dipole interactions. Interspecies scattering length a_{12} plays an essential role in the study of binary bright solitons, leading to richer dynamic phenomena.[44] Therefore, we aim to explore the influence of interspecies scattering length a_{12} on soliton properties in binary dipolar BECs. For ^{164}Dy atoms, we take $a_1 = -120a_0$, and for ^{168}Er atoms, we take $a_2 = -60a_0$, in addition set $\alpha = 1$.

3. Breathing dynamics of solitons induced by collision

Here, we use the split-step Fourier method[45] and the imaginary-time propagation method[46] to obtain the numerical profiles of bright solitons in models (3) and (4). They are denoted as $\psi_i(z)$, so the atom number of the soliton is $N_i = \int_{-\infty}^{+\infty}|\psi_i(z)|^2\mathrm{d}z$. With the chemical potential μ, the bright soliton solution in the models (3) and (4) can be written as

$$\begin{bmatrix}\Psi_1(z,t)\\ \Psi_2(z,t)\end{bmatrix} = \begin{bmatrix}\Psi_{bs1}(z)\,\mathrm{e}^{-\mathrm{i}\mu_1 t}\\ 0\end{bmatrix}, \tag{5}$$

$$\begin{bmatrix}\Psi_1(z,t)\\ \Psi_2(z,t)\end{bmatrix} = \begin{bmatrix}0\\ \Psi_{bs2}(z)\,\mathrm{e}^{-\mathrm{i}\mu_2 t}\end{bmatrix}, \tag{6}$$

It is an effective method to investigate the dynamic characteristics of solitons by the collision between solitons. We give the initial conditions for two solitons with opposite velocities

$$\begin{bmatrix}\Psi_1(z,0)\\ \Psi_2(z,0)\end{bmatrix} = \begin{bmatrix}\Psi_{bs1}(z-z_0)\\ 0\end{bmatrix}\mathrm{e}^{\mathrm{i}vz} + \begin{bmatrix}0\\ \Psi_{bs2}(z+z_0)\end{bmatrix}\mathrm{e}^{-\mathrm{i}vz}, \tag{7}$$

where $z_0 > 0$ and $v \geq 0$ are the initial offset and velocity of solitons, respectively.

We consider the case of the attractive dipole interaction (intraspecies and interspecies) and attractive contact interaction (intraspecies and interspecies). We can obtain stable bright solitons and BECs in a reasonable research range. In the numerical simulation, we adopt the split-step Fourier method to implement the amplitude evolution $|\psi(z,t)|$. Here, Figs. 1(a1)–1(c1) represent the first component and Figs. 1(a2)–1(c2) represent the second component. The initial parameters are $a_{12} = -60a_0$, $N_1 = 1$, $N_2 = 2$, $z_0 = 5$, $v = 0.8$ and the plot of amplitude evolution of the first component is illustrated in Fig. 1(a1). The result reveals that an SS structure is observed on the left side of the z-axis after the collision, and a TS structure with a stable breathing frequency is formed on the right side. Meanwhile, the plot of amplitude evolution of the second component is depicted in Fig. 1(a2), the TS structure is formed on the left side of the z-axis after collision, and the SS structure is observed on the right side. Here, we distinguish the difference between the TS structure and the SS structure based on the variation in their peak amplitude. The TS structure exhibits peak amplitude oscillations in the center, whereas, for the SS structure, the peak amplitude oscillates around the center in a snake pattern. They all have a stable breathing frequency. Then, we consider the initial parameters of $a_{12} = -60a_0$, $N_1 = 3$, $N_2 = 1$, $z_0 = 5$, $v = 0.6$, and the amplitude evolution $|\psi_1(z,t)|$ of the first component is shown in Fig. 1(b1). After the collision, we observe the SS structure on the left side of the z-axis, and the TS structure on the right side. However, due to the first component having a larger number of atoms, it can maintain stability more effectively after collision, resulting in a relatively small and inconspicuous SS structure. The amplitude evolution $|\psi_2(z,t)|$ of the second component is shown in Fig. 1(b2), we observe the TS structure on the left side of the z-axis after collision, and a unique DS structure appears on the right side. When the initial parameters are $a_{12} = -100a_0$, $N_1 = 0.5$, $N_2 = 1$, $z_0 = 5$, $v = 0.6$, the amplitude evolution $|\psi_1(z,t)|$ of the first component is shown in Fig. 1(c1). We find that the DS structure can converge to form an SS structure over time, appearing on the left side of the z-axis after collision. And the TS structure forms on the right side. This mixed breathing structure is called the MS structure. There is a TS structure on the left side of z-axis after collision and an SS structure on the right side of the second component, as shown in Fig. 1(c2).

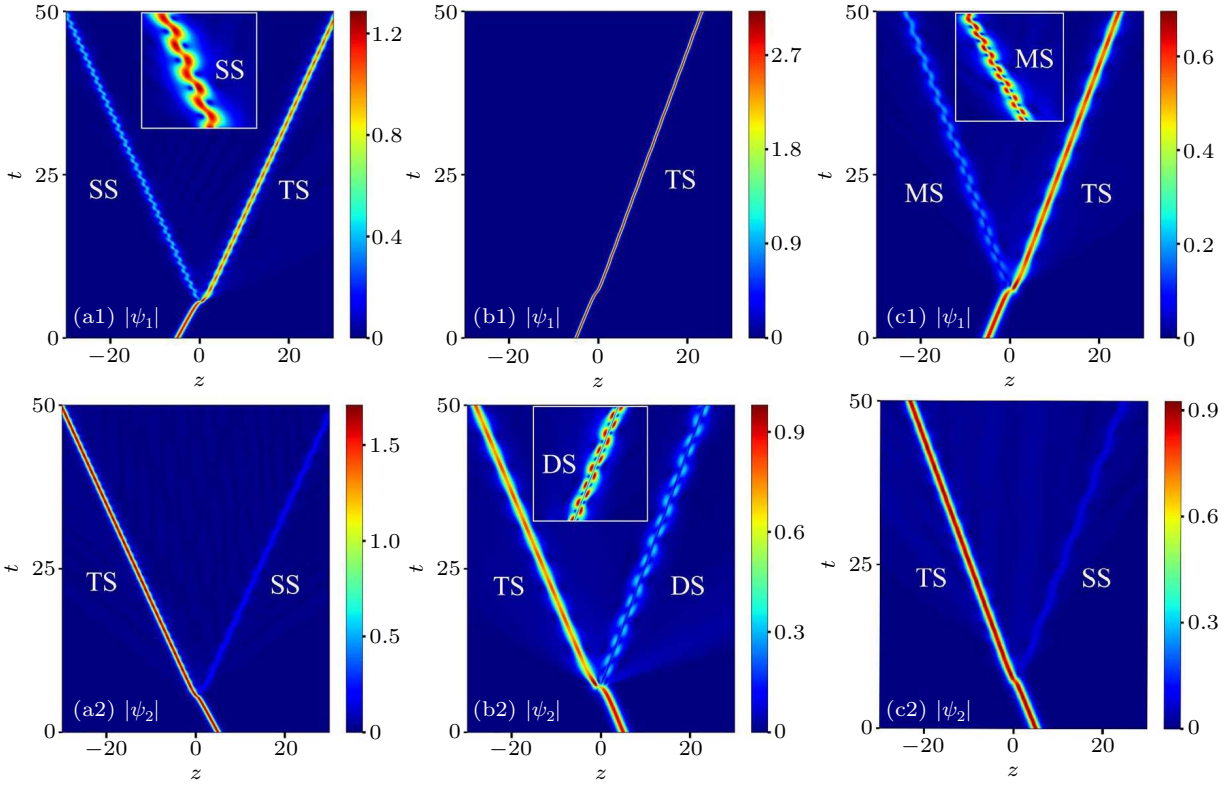


Fig. 1. The amplitude evolution plot in different components under initial conditions (7) with the following parameters: (a1) and (a2) $N_1 = 1$, $N_2 = 2$, $a_{12} = -60a_0$, $v = 0.8$; (b1) and (b2) $N_1 = 3$, $N_2 = 1$, $a_{12} = -60a_0$, $v = 0.6$; (c1) and (c2) $N_1 = 0.5$, $N_2 = 1$, $a_{12} = -100a_0$, $v = 0.6$. The upper panel indicates the first component $|\psi_1|$, the lower panel represents the second component $|\psi_2|$, and the other parameter is $z_0 = 5$.

Up to now, we have obtained three special breathing structures by simulating the collision of two bright solitons in binary dipole BECs, in which SS structure, MS structure and DS structure all exist rely on the TS structure. In this paper, we mainly excite three special breathing structures, which bring some novel breathing dynamics. Next, we will explore the conditions under which these breathing structures are excited.

To investigate the special breathing structures, we present phase diagrams in a space defined by atomic number N_i and interspecies scattering length a_{12}. Specifically, Figs. 2(a) and 2(c) are associated with the left side of the z-axis after collision, while Figs. 2(b) and 2(d) correspond to the right side of the z-axis. When the number of ^{164}Dy atom $N_1 = 1$, Fig. 2(a) shows the distribution of breathing structures for different N_2 and a_{12}. Here, the red region corresponds to the excitation of SS and TS structures (first and second components), while the blue region corresponds to the excitation of MS and TS structures (first and second components). Furthermore, in Fig. 2(b), we give the excitation conditions of TS and DS structures (first and second components) in the green area and ones of TS and SS structures (first and second components) in the red area. It is evident from Figs. 2(a) and 2(b) that the quasi-transition between different types of special structures is dependent on the atomic number N_i and the interspecies scattering length a_{12}. In the quasi-transition process, the atomic number N_i plays a more important role. The result indicates that when the atomic number of the second component is larger than that of the first component, a stable SS structure in the first component can gradually separate into MS structures. And the divided DS structures in the second component can gradually turn into stable SS structures.

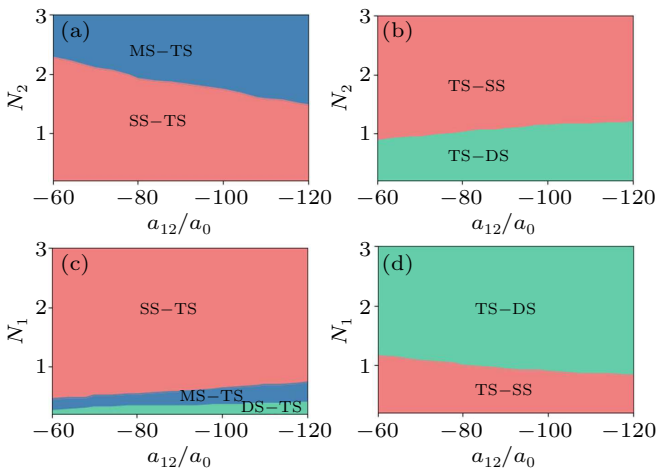


Fig. 2. The phase diagrams depict the special breathing structure observed after a collision between binary ^{164}Dy–^{168}Er solitons. When $N_1 = 1$, (a) and (b) depict the special breathing structures that are respectively excited on the left and right sides following the collision along the z-axis. When $N_2 = 1$, (c) and (d) depict the special breathing structures that are respectively excited on the left and right sides following the collision along the z-axis. The front of the bar indicates the first component, and the back of the bar indicates the second component. The parameters used in the numerical simulation are $a_1 = -120a_0$, $a_2 = -60a_0$, $v = 0.6$, $z_0 = 5$.

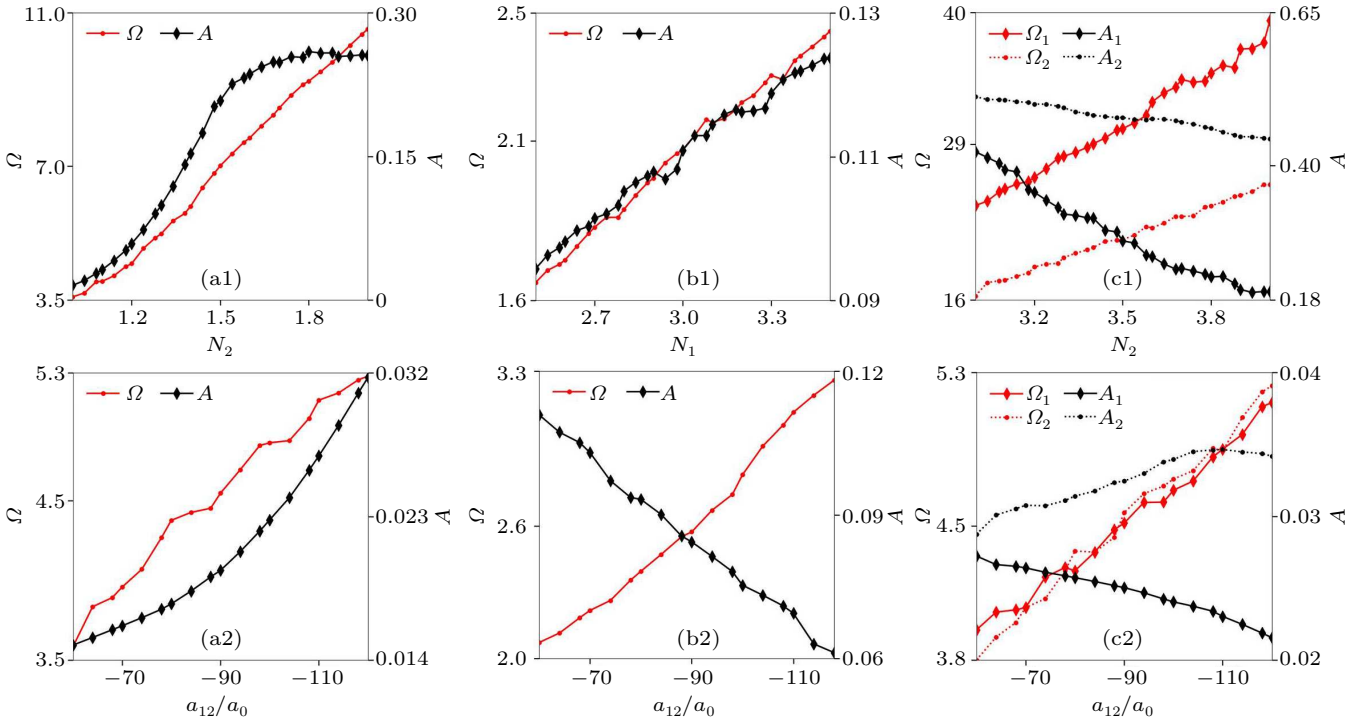


Fig. 3. Effect of atomic number N_i and interspecies scattering length a_{12} on the maximum value of the breathing amplitude A and frequency Ω of three breathing structures: SS, DS, MS (from left to right). The initial condition for panel (a1) $N_1 = 1$, $a_{12} = -60a_0$, panel (b1) $N_2 = 1$, $a_{12} = -60a_0$, panel (a2) $N_1 = 1$, $N_2 = 2$, panel (b2) $N_1 = 3$, $N_2 = 1$, where the solid red line indicates the breathing frequency Ω, and the solid black line indicates the maximum value of the breathing amplitude A. In panel (c1) $N_1 = 1$, $a_{12} = -100a_0$ and in panel (c2) $N_1 = 0.4$, $N_2 = 1$, where the solid red and black lines represent breathing frequency Ω_1 and the maximum value of the breathing amplitude A_1 before mixing, respectively, and the red and black dashed lines represent the breathing frequency Ω_2 and the maximum value of the breathing amplitude A_2 after mixing, respectively. The other parameters are $z_0 = 5$, $v = 0.6$.

When the number of ^{168}Er atom $N_2 = 1$, in Fig. 2(c), the green area excites DS and TS structures (first and second components), the blue area excites MS and TS structures (first and second components), and the red area excites SS and TS structures (first and second components). As the atomic number N_1 increases, the quasi-transition from DS structure to MS structure to SS structure can be achieved in the first component. In Fig. 2(d), the red region excites the TS and SS structures (the first and second components) and the green region excites the TS and DS structures (the first and second components). As the atomic number N_1 increases, the quasi-transition from the SS structure to the DS structure can be achieved in the second component.

It can be seen from Fig. 2 that atomic number N_i and interspecies scattering length a_{12} have significant effects on the three breathing structures. The character of the breathing structure can be described by its maximum breathing amplitude A and breathing frequency Ω. We define the time when peak appears as t_{peak}. In the numerical simulation, the breathing period T_{br} can be measured by the average value of time differences between two adjacent peaks of $|\psi(z_{\text{m}},t)|^2$, i.e., the average value of $t_{\text{peak}}^{(n)} - t_{\text{peak}}^{(n+1)}$. Thus, the breathing frequency is $\Omega_{\text{br}} = 2\pi/T_{\text{br}}$. The maximum breathing amplitude A_{br} can be measured by the average value of $|\psi(z_{\text{m}},t)|^2$ of all peaks, i.e., $A_{\text{br}} = \sum_n |\psi(x_{\text{m}},t_{\text{peak}}^{(n)})|^2/n$.

In the case where $a_{12} = -60a_0$, $N_1 = 1$, our findings indicate that the maximum breathing amplitude A and frequency Ω of the SS structure increase as N_2 increases, as shown in Fig. 3(a1). Additionally, when $N_1 = 1$, $N_2 = 2$, the maximum breathing amplitude A and frequency Ω of the SS structure increase with increasing interspecies scattering length a_{12}, as demonstrated in Fig. 3(a2). Therefore, we manipulate the maximum breathing amplitude A and frequency Ω of the SS structure by atomic number N_i and interspecies scattering length a_{12}. As mentioned earlier, the DS structure comprises two columns of breathing solitons that are nearly identical. So, the maximum breathing amplitude A and breathing frequency Ω of DS structure are described by the average of the two columns of breathing solitons. In the scenario where $a_{12} = -60a_0$, $N_2 = 1$, the findings indicate that the maximum breathing amplitude A and breathing frequency Ω of the DS structure increase with increasing N_1, as illustrated in Fig. 3(b1). Conversely, in the case of $N_1 = 3$, $N_2 = 1$, the maximum breathing amplitude A of the DS structure gradually decreases with increasing interspecies scattering length a_{12}, while the breathing frequency Ω gradually increases, as demonstrated in Fig. 3(b2). Furthermore, we have a new discovery for the MS structure, which is comparable to the quasi-transition stage of divided DS structure turning into an SS structure. Therefore, the MS structure research is divided into

two categories: pre-mixing and post-mixing. During numerical simulations, we designate the collision time point as the initial time, pre-mixing as the time period from 0 to 10, and post-mixing as the time period from 50 to 60. A_1, A_2, Ω_1, and Ω_2 represent the maximum breathing amplitude and frequency before and after mixing, respectively. For $a_{12} = -100a_0$, $N_1 = 1$, the results indicate that as N_2 increases, the maximum breathing amplitudes (A_1 and A_2) of the MS structure before and after mixing gradually decrease, while the breathing frequencies (Ω_1 and Ω_2) before and after mixing progressively increase, as illustrated in Fig. 3(c1). In the case where $N_1 = 0.4$, $N_2 = 1$, the findings indicate that with increasing interspecies scattering length a_{12}, the maximum breathing amplitude A_1 of the MS structure before mixing gradually decreases, while the maximum breathing amplitude A_2 after mixing gradually increases. Moreover, the breathing frequency (Ω_1 and Ω_2) before and after mixing progressively increases, as illustrated in Fig. 3(c2).

When studying the breathing character of the MS structure, we find that the lifetime τ of the MS structure is influenced by atomic number N_i and interspecies scattering length a_{12}.

We aim to quantitatively investigate the relation between the lifetime τ of the MS structure and the atomic number N_i and the interspecies scattering length a_{12}. During numerical simulations, we utilize the following initial conditions for the collision of two solitons: $N_1 = 0.5$, $N_2 = 1$, $a_{12} = -100a_0$, $v = 0.6$, $z_0 = 5$. Furthermore, we capture the dip profile of the MS structure in the first component and the TS structure in the second component at $t = 20$ in the real-time evolution process. Their initial expressions are as follows: $\begin{bmatrix} \psi_{\rm br1}(z) \\ \psi_{\rm br2}(z) \end{bmatrix}$. It is obtained after the soliton center at the inclination moves to the coordinate origin and only the amplitude distribution is preserved. Subsequently, by integrating the modulus of the centroid coordinates, the P-value is obtained, which is a physical quantity describing the lifetime τ of the MS structure. The integral expression of P is denoted by

$$P = \int_{t-t_0}^{t+t_0} |\bar{z}|t \, \mathrm{d}t, \quad \bar{z} = \frac{\int_l z|\psi_{\rm br1}(z)|^2 \mathrm{d}l}{\int_l |\psi_{\rm br1}(z)|^2 \mathrm{d}l},$$

where $\bar{z}$ represents the centroid coordinates.

The outcomes depicted in Fig. 4(b) demonstrate that the centroid coordinates gradually approach the 0-axis over time. To determine the lifetime τ, we refer to the amplitude evolution diagram of the MS structure displayed in Fig. 4(a) and integrate the centroid coordinates to obtain a reasonable threshold. During the numerical simulations, we set the time precision to $\Delta t = 0.002$ and the time interval to $t_0 = 3$. Based on statistical analysis, we confirm that when $P < 1.6$, a mixed state is reached. In Fig. 4(c), we observe that the lifetime τ decreases as the atomic number N_1 increases when $N_2 = 1$, $a_{12} = -100a_0$. In Fig. 4(d), we demonstrate that an increase in the interspecies scattering length a_{12} results in an increase in the lifetime τ, when $N_1 = 0.5$, $N_2 = 1$.

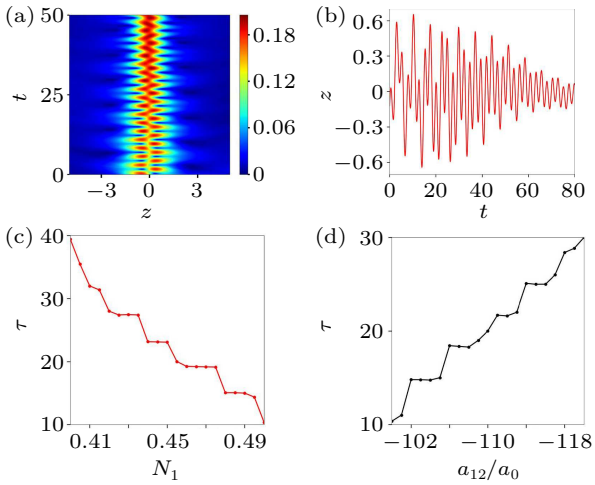


Fig. 4. When $N_1 = 0.5$, $a_{12} = -100a_0$, $N_2 = 1$, (a) amplitude evolution plot of MS structure and (b) the centroid coordinate plot corresponding to the MS structure amplitude evolution plot. (c) The variation in lifetime with the atomic number N_1 when $a_{12} = -100a_0$, $N_2 = 1$. (d) The variation in lifetime with the interspecies scattering length a_{12} when $N_1 = 0.5$, $N_2 = 1$.

4. Interaction between three special breathing structures

We have successfully induced three unique breathing structures through the collision of bright solitons, resulting in rich breathing dynamics. Next, we want to explore the interactions among these distinctive breathing structures. In numerical simulations, we apply the super-Gaussian function to filter the dip profile and weaken the radiation waves outside the soliton to better illustrate the collision dynamics. Consequently, the initial condition is changed into

$$\begin{bmatrix} \Psi_1(z,0) \\ \Psi_2(z,0) \end{bmatrix} = \begin{bmatrix} \Psi_{\rm br1}^{(l)}(z-z_0) \\ \Psi_{\rm br2}^{(l)}(z-z_0) \end{bmatrix} \mathrm{e}^{\mathrm{i}vz} + \begin{bmatrix} \Psi_{\rm br1}^{(k)}(z+z_0) \\ \Psi_{\rm br2}^{(k)}(z+z_0) \end{bmatrix} \mathrm{e}^{-\mathrm{i}vz}. \quad (8)$$

The above initial conditions include three special breathing structures, such as SS structures, DS structures and MS structures. They are both made up of medial peaks and lateral peaks. As shown in the Fig. 5(a) for MS structure, the peak near the 0-axis is the medial peak, and the one far away from the 0-axis is the lateral peak, denoted as M and L respectively. The result reveals that the collision between two identical SS or DS structures does not change their respective breathing types. In other words, they remain as SS or DS structures after collision. However, when two identical MS structures collide, it significantly impacts their breathing properties. For instance, the collision can lead to changes in their lifetime. Based on the findings displayed in Fig. 5(a), it is evident that two MS structures can sustain their individual type for an

extended period after collision, indicating a longer lifetime. However, from Fig. 5(b), it is observed that two MS structures collide and rapidly transform into SS structures, implying a shorter lifetime. The difference in velocity under the initial conditions is responsible for this result. Consequently, we utilize the collision time t_c to describe the effect of velocity on its lifetime τ. Next, we explore the relationship between the lifetime τ of MS structures and the collision time t_c. During the numerical evolution, the time period of both medial and lateral peaks is denoted as $T_{DS} = 1.33$. The research results, as shown in Fig. 5(c), indicate that collisions play a crucial role in the lifetime of MS structure, and its lifetime presents a periodic change with t_c. Subsequent to the collision, the SS structure formation time period is approximately $T_{SS} = 1.4$, whereas the MS structure formation time period is about $T_{MS} = 1.3$. From the figure, it is evident that the maximum lifetime of the MS structure post-collision consistently falls within the interval spanning from M to L. The collision between two different breathing structures can also alter the breathing types and breathing properties of the SS structure, MS structure, and DS structure. Collisions at different velocities can result in mutual transformations among these three special breathing structures, namely the SS structure, MS structure, and DS structure.

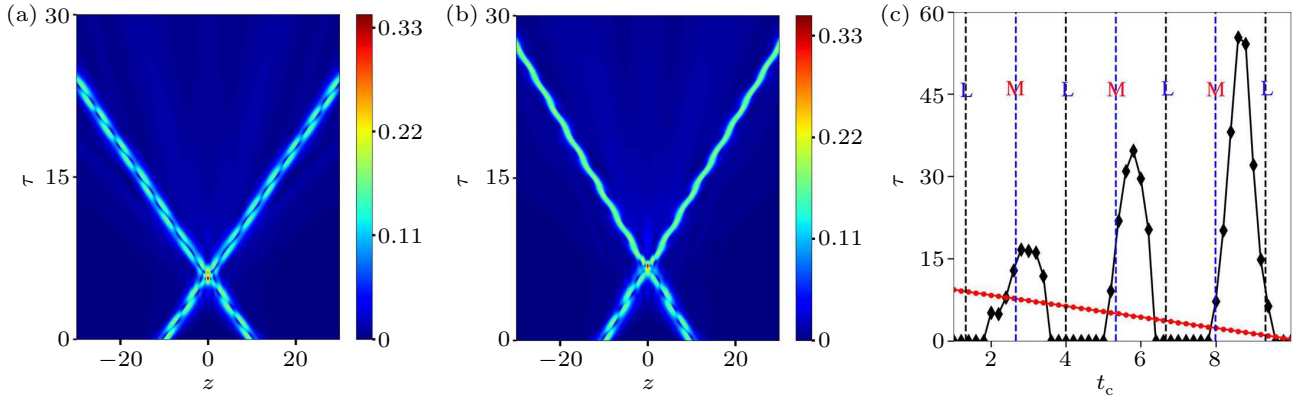


Fig. 5. When $N_1 = 0.5$, $N_2 = 1$, $a_{12} = -100a_0$, $z_0 = 10$, the amplitude evolution plots for the collision of two MS structures at time (a) $t_c = 6$, and (b) $t_c = 7$. (c) The variation of the lifetime τ of MS structures after collision with respect to the collision time t_c. The black solid line represents the lifetime τ of the MS structure after collision, and the solid red line represents the lifetime τ of the MS structure without interaction.

5. Conclusion

We conduct numerical studies on the collision process of bright solitons in a binary dipolar BECs system. The breathing phenomenon of solitons after collision is caused by the attractive dipole–dipole interaction and contact interaction. After the collision, we obtain three special breathing structures, such as SS structure, MS structure, and DS structure. The characteristics of these breathing structures can be described by breathing frequency Ω, maximum breathing amplitude A and lifetime τ, which can be manipulated by atomic number N_i and interspecies scattering length a_{12}. Meanwhile, the above-mentioned breathing structures can undergo quasi-transition processes through appropriate choices of N_i and a_{12}. Additionally, the collision of two identical special breathing structures also can bring more abundant breathing dynamics. The results show that two SS or DS structures of the same type can maintain their stability after collision, while the collision of two identical MS structures at different velocities can either extend or shorten their lifetime τ. Our findings indicate significant differences from the single-component dipolar BECs, thereby enriching the collision dynamics of matter-wave solitons. Furthermore, Our results provide a reference for the study of soliton interactions and deepen the understanding of soliton properties in a binary dipolar BECs.

Acknowledgment

Project supported by the National Natural Science Foundation of China (Grant Nos. 12247103, 12275213, and 12247110).

References

[1] Achilleos V, Frantzeskakis D J, Kevrekidis P G, *et al.* 2013 *Phys. Rev. Lett.* **110** 264101
[2] Nguyen J, Dyke P, Luo D, *et al.* 2014 *Nat. Phys.* **10** 918
[3] Zabusky N J and Kruskal M D 1965 *Phys. Rev. Lett.* **15** 240
[4] Matveev V B and Salle M A 1991 *Darboux Transformations and Solitons* (Berlin: Springer)
[5] Akhmediev N and Ankiewicz A 1993 *Opt. Commun.* **100** 186
[6] Zhao L C, Ling L, Yang Z Y, *et al.* 2016 *Nonlinear Dyn.* **83** 659
[7] Zhao L C, Ling L, Yang Z Y, *et al.* 2017 *Nonlinear Dyn.* **88** 2957
[8] Kumar V R, Radha R and Panigrahi P K 2009 *Phys. Lett. A* **373** 4381
[9] Lu M W, Burdick N Q, Youn S H, *et al.* 2011 *Phys. Rev. Lett.* **107** 190401
[10] Aikawa K, Frisch A, Mark M, *et al.* 2012 *Phys. Rev. Lett.* **108** 210401
[11] Tang Y J, Burdick N Q, Baumann K, *et al.* 2015 *New J. Phys.* **17** 045006
[12] Beaufils Q, Zanon T, Chicireanu R, *et al.* 2008 *Phys. Rev. A* **78** 051603
[13] Griesmaier A, Werner J, Hensler S, *et al.* 2005 *Phys. Rev. Lett.* **94** 160401
[14] Stuhler J, Griesmaier A, Koch T, *et al.* 2005 *Phys. Rev. Lett.* **95** 150406
[15] Pedri P and Santos L 2005 *Phys. Rev. Lett.* **95** 200404

[16] Dauxois T, Ruffo S, Arimondo E, *et al.* 2002 *Dynamics and Thermodynamics of Systems with Long-Range Interactions* (Berlin: Springer)
[17] Giovanazzi S, Görlitz A and Pfau T 2002 *Phys. Rev. Lett.* **89** 130401
[18] Sinha S and Santos L 2007 *Phys. Rev. Lett.* **99** 140406
[19] Frantzeskakis D J and Carretero-González R 2008 *Emergent nonlinear phenomena in Bose–Einstein condensates: theory and experiment* (Berlin: Springer)
[20] Koch T, Lahaye T, Metz J, *et al.* 2008 *Nat. Phys.* **4** 218
[21] Lahaye T, Metz J, Froehlich B, *et al.* 2008 *Phys. Rev. Lett.* **101** 080401
[22] Lahaye T, Menotti C, Santos L, *et al.* 2009 *Rep. Prog. Phys.* **72** 126401
[23] Baizakov B B, Al-Marzoug S M and Bahlouli H 2015 *Phys. Rev. A* **92** 033605
[24] Turmanov B K, Baizakov B B, Umarov B A, *et al.* 2015 *Phys. Lett. A* **379** 1828
[25] Pawłowski K and Rzążewski K 2015 *New J. Phys.* **17** 105006
[26] Edmonds M J, Bland T, O'Dell D H J, *et al.* 2016 *Phys. Rev. A* **93** 063617
[27] Raghunandan M, Mishra C, Łakomy K, *et al.* 2015 *Phys. Rev. A* **92** 013637
[28] Tikhonenkov I, Malomed B A and Vardi A 2008 *Phys. Rev. A* **78** 043614
[29] Strecker K E, Partridge G B, Truscott A G, *et al.* 2002 *Nature* **417** 150
[30] Khaykovich L, Schreck F, Ferrari G, *et al.* 2002 *Science* **296** 1290
[31] Liu W M, Kengne E, Liu W M, *et al.* 2019 *Nonlinear Schrödinger Equations of Single Transmission Lines* (Berlin: Springer)
[32] Kengne E, Liu W M and Malomed B A 2021 *Phys. Rep.* **899** 1
[33] Wen L, Guo H, Wang Y J, *et al.* 2020 *Phys. Rev. A* **101** 033610
[34] Zhang X F, Hu X H, Liu X X, *et al.* 2009 *Phys. Rev. A* **79** 033630
[35] Perez-Garcia V M and Beitia J B 2005 *Phys. Rev. A* **72** 033620
[36] Adhikari S K 2005 *Phys. Lett. A* **346** 179
[37] Öhberg P and Santos L 2001 *Phys. Rev. Lett.* **86** 2918
[38] Morera I, Mateo A M, Polls A, *et al.* 2018 *Phys. Rev. A* **97** 043621
[39] Young S L E and Adhikari S K 2013 *Phys. Rev. A* **87** 013618
[40] Adhikari S K and Young S L E 2010 *J. Phys. B* **47** 015302
[41] Deuretzbacher F, Cremon J C and Reimann S M 2010 *Phys. Rev. A* **81** 063616
[42] Inouye S, Andrews M R, Stenger J, *et al.* 1998 *Nature* **392** 151
[43] Blatt S, Nicholson T L, Bloom B J, *et al.* 2011 *Phys. Rev. Lett.* **107** 073202
[44] He Z M, Wang D L, Ding J W, *et al.* 2012 *Eur. Phys. J. D* **66** 1
[45] Yang J 2010 *Nonlinear Waves in Integrable and Nonintegrable Systems* (Philadelphia: SIAM)
[46] Muruganandam P and Adhikari S K 2009 *Comput. Phys. Commun.* **180** 1888